Lecture 23
Magnetic Fields, Core Stability and Collapse

1. Magnetic Fields and Stability
2. Singular Isothermal Sphere
3. Observational Signatures of Infall

References

McKee, Lec22-06 & OSSP (Crete 1999)
Stahler, Chs. 9 & 10
Shu, ApJ 214 488 1977
Troland & Crutcher (2008)

1. Magnetic Fields and Stability

- Observations show that GMCs are large (10-100 pc), cold (~ 20 K), fairly dense (~ 10^2 - 10^3 cm^{-3}), and turbulent (Δv ~ 1 km s^{-1}) ***gravitationally bound*** overall***.***

- More detailed observations show that they contain small (~ 0.1 pc), cold (~ 10 K), dense (~ 10^3 - 10^5 cm^{-3}) and often turbulent regions called ***cloud cores*** that are also bound, but perhaps not always gravitationally.

- But the cores may also contain newly formed stars and thus manifest both stability and instability although on different spatial scales. To explore this situation, we further examine the stability of molecular clouds and especially the role of ***magnetic fields***.

The First Stability Results

Without magnetic fields, we found that the conditions for ***gravitational instability*** (collapse) can be given in terms of certain quantities like the Jeans length, time, and mass. They are determined solely by two parameters: the dispersion in the ***random velocity*** that determines the effective gas pressure and the average ***mass density*** of the cloud that determines the effects of gravity:

$$c^2 = \frac{kT}{m} + \sigma_{\rm turb}{}^2$$

and, for no turbulence,

$$\lambda_{\rm J} = c\sqrt{\frac{\pi}{G\rho}} = 0.189\,{\rm pc}\left(\frac{10{\rm K}}{T}\right)^{1/2}\left(\frac{1}{n({\rm H}_2)}\right)^{-1/2}$$

$$M_{\rm J} = \lambda_{\rm J}{}^3\rho = 4.79 M_{\rm sun}\left(\frac{10{\rm K}}{T}\right)^{3/2}\left(\frac{1}{n({\rm H}_2)}\right)^{-1/2}$$

Stable and Unstable Virial Equilibrium

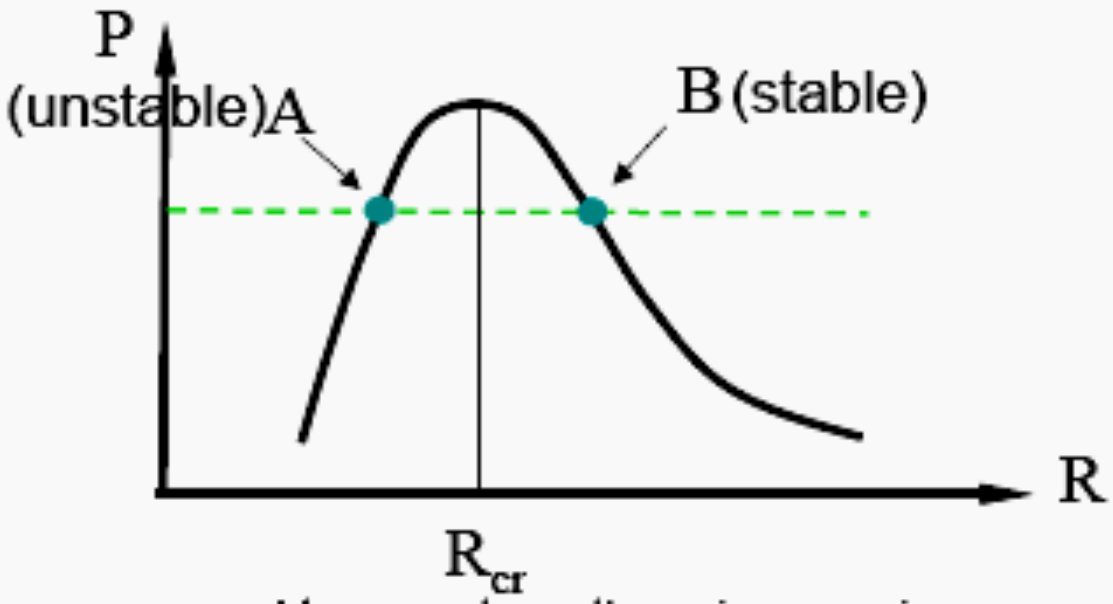

For a given mass and temperature, there is a maximum pressure for stability. Alternatively, given a value of the external pressure, there is a maximum stable mass. The solution of the Lane-Emden equation by Bonnor (MNRAS 116 351 1956) & Ebert (Zs. f. Ap 37 222 1955) gives the critical mass as

$$M_{cr} \cong 1.2 \frac{c^4}{G^{3/2} P_{ext}} = O(M_J)$$

Virial Analysis of a Magnetized Cloud

Apply the virial theorem from Lec22 for an equilibrium cloud

$$P_{\rm ext}\,V-\langle P\rangle\,V=\frac{2}{3}E_{\rm K}+\frac{1}{3}W+\frac{1}{3}M$$

Ignore rotation and turbulence (E_K - 0) and focus on the last (magnetic) term. In the spirit of the approximations in Lec22, assume

1. The magnetization is uniform,
2. The field outside is dipolar
3. Magnetic flux is conserved, $\Phi \approx \pi R^2 B$, I.e., the cloud is a sufficiently good conductor to allow flux-freezing

$$4\pi R^3 P = 3c^2 M - \frac{3}{5}\frac{GM^2}{R} + \frac{1}{3}R^3 B^2$$

$$= 3c^2 M - \frac{3}{5}\frac{GM^2}{R} + \frac{1}{3\pi^2}\frac{\Phi^2}{R}$$

Virial Analysis for a Magnetized Cloud

$$P = \frac{3}{4\pi}\frac{Mc^2}{R^3} - \frac{3}{20\pi}\frac{GM^2}{R^4} + \frac{1}{12\pi^3}\frac{\Phi^2}{R^4}$$

The magnetic and gravitational energies vary with R in the same way.

Since they stand in a constant ratio, once a cloud starts collapsing the frozen-in magnetic field cannot stop it.

Magnetically dominated clouds are stable, i.e, clouds whose mass is less than the value:

$$M_\Phi \equiv \frac{1}{\pi}\left(\frac{5}{9G}\right)^{1/2}\Phi$$

More careful analysis, originally due to Mouschovias & Spitzer (ApJ 210 326 1974) leads to the slightly more accurate formula,

$$M_\Phi \approx 0.13\, G^{-1/2}\Phi = 1.0 M_{\rm sun}\left(\frac{B}{20\mu{\rm G}}\right)\left(\frac{R}{0.1\,{\rm pc}}\right)^2$$

NB In some papers, 0.13 is replaced by $1/2\pi$ in the last formula.

Magnetically Critical Mass

This analysis leads to the following terminology:

- *Magnetically Sub-Critical Mass*: $M < M_{\Phi}$ - Magnetism stronger than gravity. The external pressure maintains the cloud in equilibrium but does not collapse it.
- *Magnetically Super-Critical Mass*: $M > M_{\Phi}$ - Magnetism weaker than gravity. The external pressure aids collapse.

The virial equation can be rewritten in terms of $M_{\Phi:}$

$$P = \frac{3}{4\pi}\frac{Mc^2}{R^3} - \frac{3}{20\pi}\frac{G}{R^4}(M^2 - M_{\Phi}{}^2)$$

Measurements of magnetic fields in cores (Troland and Crutcher (2008; slides 10 & 11) Indicate that they are often on the margin between sub and super critical.

The Fate of Sub-Critical Cores

- Sub-critical cores may collapse on long timescales via ***ambipolar diffusion*** (see Shu II, Ch. 27).
- Gravity acts on all of the components of the interstellar cloud, ions as well as neutrals (the dominant component).
- But the ions are tied to the magnetic field; they tend to force the neutrals to follow them by microscopic ion-neutral interactions.
- Over time, however, gravity drags the neutrals through the ions and feeds the center of the collapse.
- The drift speed varies inversely with the electron fraction, so ambipolar diffusion is faster inside a core compared to its surface
- Alternatively, gas dynamic forces in a ***turbulent cloud*** may drive a cloud core into collapse

Ambipolar Diffusion Timescale

Assuming ideal MHD, the force per unit volume is balanced by the drag force,

$$\frac{1}{4\pi}(\nabla \times \vec{B}) \times \vec{B} = \frac{m_i m_n}{m_i + m_n} K\, n_i n_n\, \vec{w}$$

where *i* and *n* stand for ions and neutrals, *K* is the rate coefficient for ion-neutral momentum-changing collisions, and ***w*** is the drift velocity of interest. One can easily check the dimensions of the right side, and that *w* is sensitive to: B, n_H^2 and x_e.

A crude estimate, based on replacing the LHS by $B^2/4\pi L$, and using $B \sim 20$ G, $K \sim 10^{-9}$ cm^3 s^{-1}, H_2 as the neutral, and other typical core properties yields $w \ll 1$ km s^{-1}.

Core Magnetic Field Measurements

Troland & Crutcher 2008 astro-ph 0802.2253

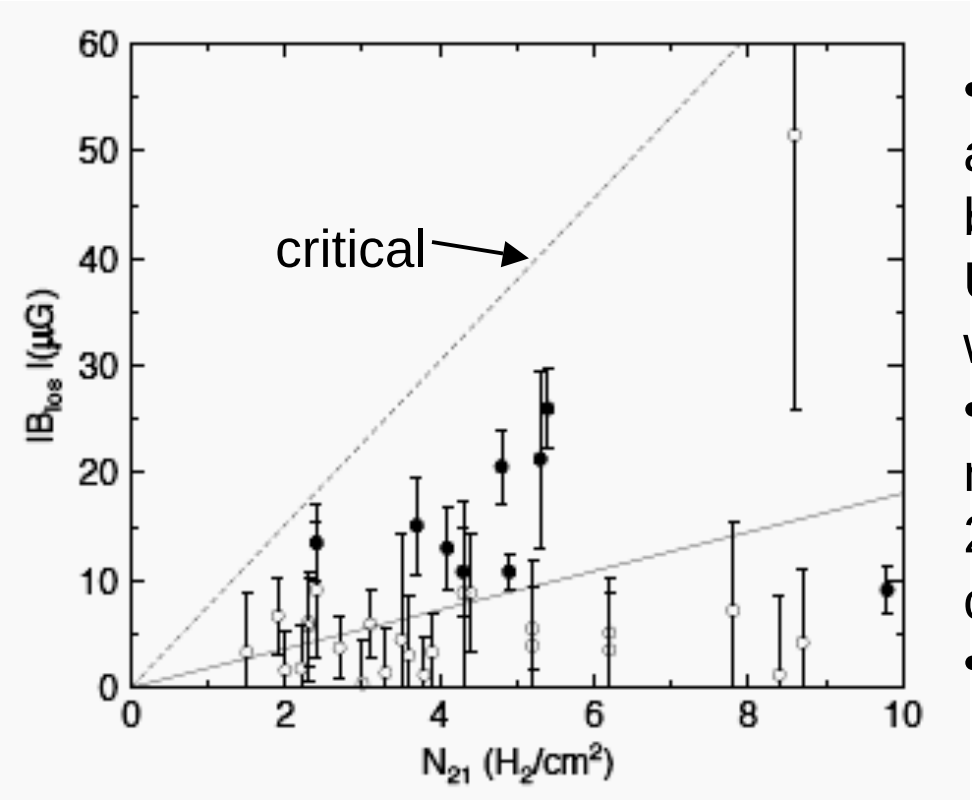

- OH Zeeman measurements are considered the most definitive, but they are notoriously difficult. Until recently, only a few results were reliable.
- Troland and Crutcher reported 9 new "probable" detections at the 2.5σ level after observing 34 dark clouds for 500 hours with Arecibo
- Error bars are 1σ!

Fig. 2.— Results for B_{los} from the Arecibo dark cloud survey plotted against the H_2 column density ($N_{21} = 10^{-21}N$). The 9 probable detections (see text) are plotted as filled circles, while non-detections are plotted as open circles. Error bars are 1σ. The solid line is the weighted mean value for the mass to flux ratio with respect to critical inferred from the Zeeman B_{los} data with no geometrical correction; $\lambda \approx 4.8 \pm 0.4$. After geometrical corrections (see text), $\lambda_c \approx 2$, or slightly supercritical. The dashed line is the critical mass to flux ratio.

OH Spectra for Troland-Crutcher Detections

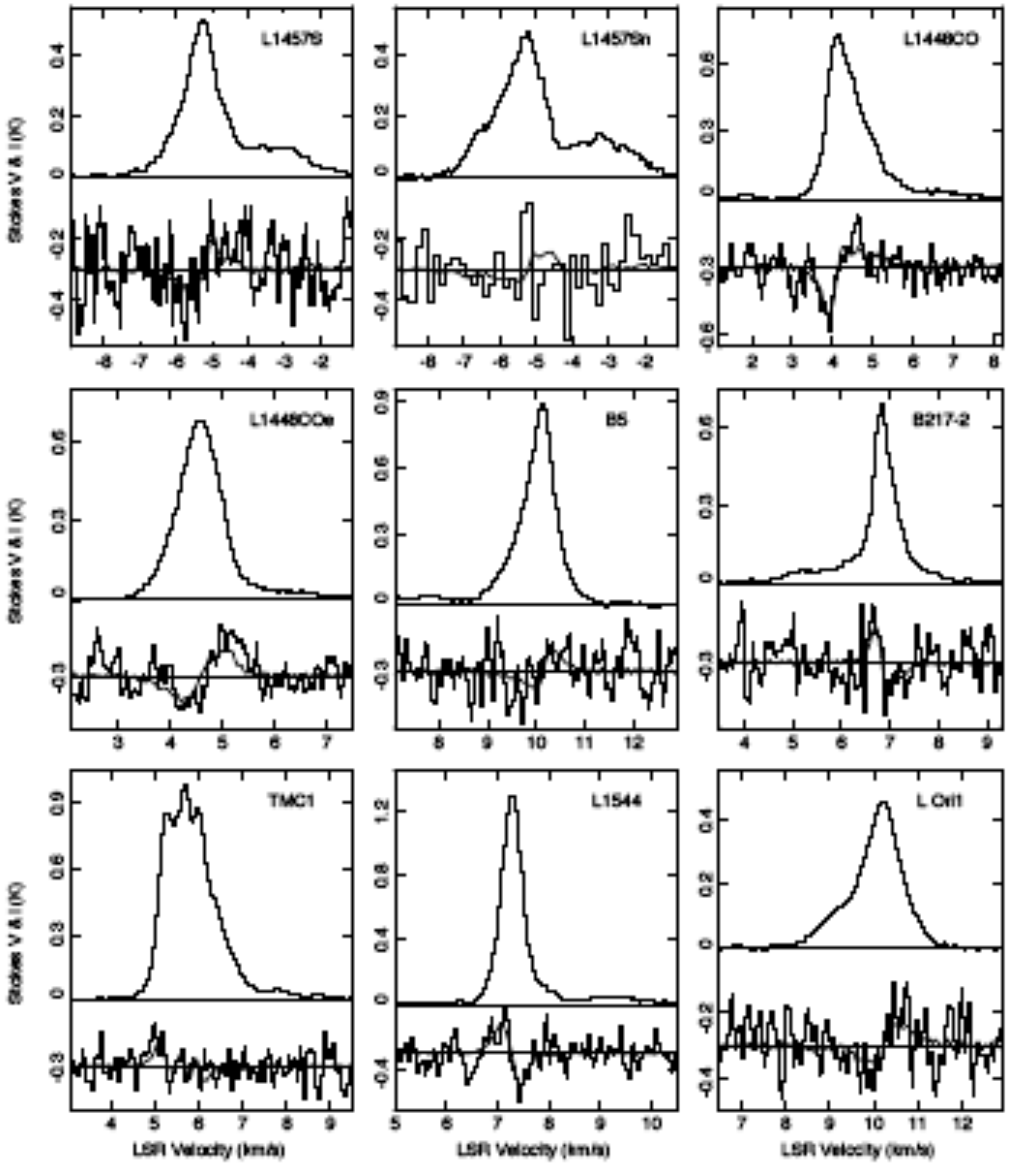

Discussion of Troland & Crutcher 2008

• Arecibo (3') observations of OH 1665, 1667 line shapes, added and subtracted to give Stokes $I(\nu)$ and $dI(\nu)/d\nu$ *for* B_{los} for 34 dark cloud cores and 9 "probable" new detections.

• Requires geometrical correction of ~ 3 to get total *B.*

• OH/H_2 assumed to be $8x10^{-8}$ to obtain H_2 column.

• Core mass = $2.8 m_H \pi R^2 N(H_2)$

• Cores are mildly supersonic: Δv_{FWHM} = 0.7 km/s; other average properties are:

$$B_{los} \sim 8\ \mu G,\ \ R \sim 0.3\ pc,\ \ N(H_2) \sim 4x10^{21} cm^{-2}$$

• Main result: $M/M_\Phi \sim 1.5$ (with geometrical correction of 3), and $E_{turb} > E_{grav} > E_{mag}$ with each ratio is ~ 2.

• Technical issues: large uncertainties (error bars), cores barely resolved in OH

• Heterogeneous sample: cores come from a variety of molecular clouds

Summary: Magnetic Fields in Dense Cores

- The observations show that magnetic fields play a significant role in molecular clouds.
- The best but still incomplete OH Zeeman measurements indicate mass-to-flux ratios the same order as critical, and even slightly larger.
- Turbulence must also play a role since the linewidths indicate that the turbulent energy is somewhat larger than the gravitational.
- Polarization maps reveal that magnetic fields threading molecular clouds are ordered over large scales.
- Magnetic fields play a role the formation of stars by shaping the structure of the clouds and cores, e.g., clouds tend to collapse preferentially along the direction of the average field.

3-D MHD Simulation of Core Formation

Li, Norman, Mac-Low & Heitsch, ApJ 605 800 2004

an alternate scenario for core formation

- 512^3 element periodic box
- super critical field
- strong supersonic turbulence
- $M = 64\ M_J$, L - $4\ L_J$
- followed for 3 free-fall times
- no microscopic physics

readily forms prolate and tri-axial super critical cores and centrifugally supported massive disks at late times (numbered in figure)

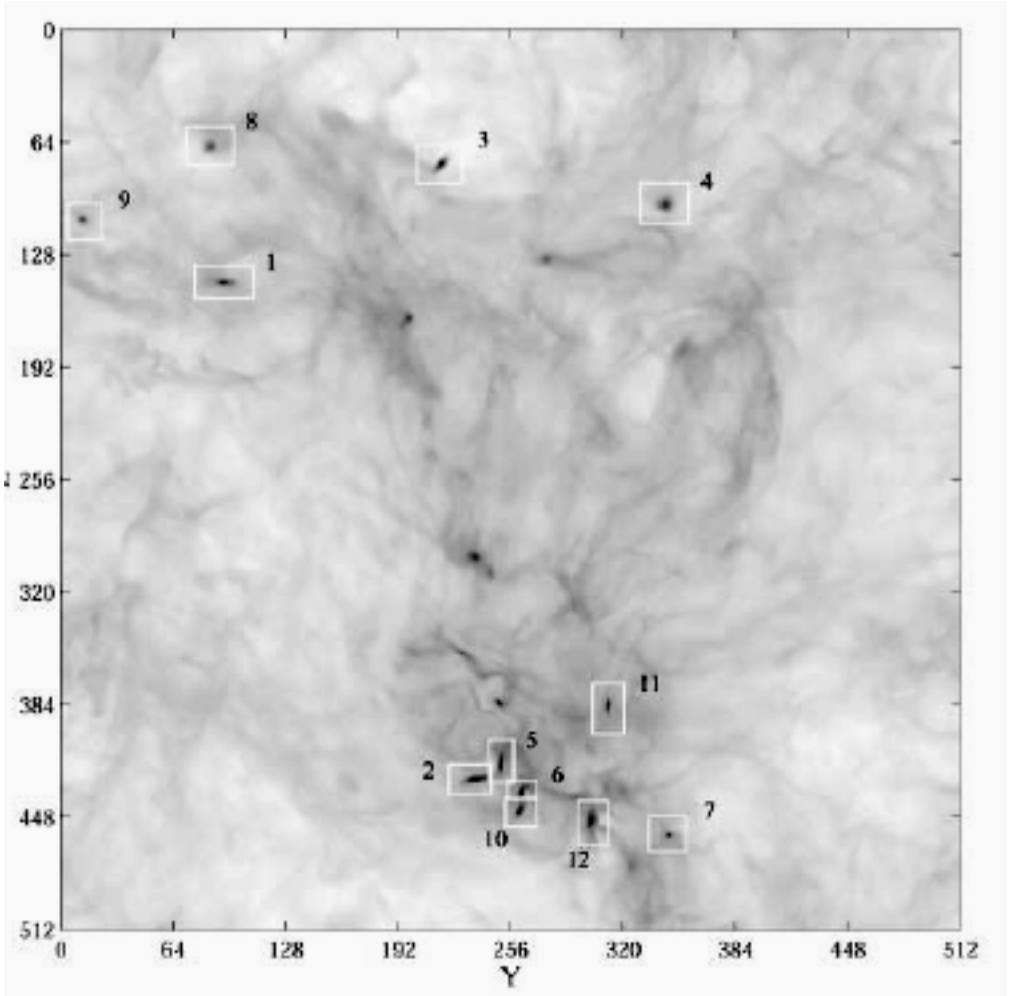

column density map with disk-like structures

2. The Singular Isothermal Sphere

We go beyond the virial analysis and try to understand how a core can appear to be both stable and collapsing by studying the Lane-Emden equation for an isothermal sphere:

$$\nabla^2\phi = 4\pi G \quad \rightarrow \quad \frac{1}{r^2}\frac{d}{dr}\left(r^2\frac{d\phi}{dr}\right) = 4\pi G$$

$$\nabla p = -\rho\nabla\phi \quad \rightarrow \quad \frac{dp}{dr} = -\rho\frac{d\phi}{dr} \quad \rightarrow \quad \frac{d\phi}{dr} = -c^2\frac{d\rho}{dr}$$

using $p = \rho c^2$. Substituting the 2nd into the 1st gives

$$\frac{1}{r^2}\frac{d}{dr}\left(r^2\frac{1}{\rho}\frac{d\rho}{dr}\right) = -\frac{4\pi G\rho}{c^2}.$$

We seek equilibrium solutions satisfying:

$$\rho'(0) = 0 \qquad \rho(R) = p_{\rm ext}c^{-2} \qquad M(r) = 4\pi\int_0^R dr\, r^2\rho(r)$$

The solutions were first studied in detail by Bonnor, Ebert and McCrea.

Bonnor-Ebert-McCrea Solutions

BEM showed that an isothermal cloud of radius R subject to an external pressure $P_{\rm ext}$ is unstable If its mass exceeds a critical value

$$M_{cr} = 1.18 \frac{c^4}{G^{3/2}} P_{\rm ext}^{-1/2}$$

Shu (ApJ 214 488 1977) noticed that the unstable solutions asymptote to a $1/r^2$ envelope, and he showed that $1/r^2$ is a particular (singular) solution of the BEM Eq., which he described as the "singular isothermal sphere".

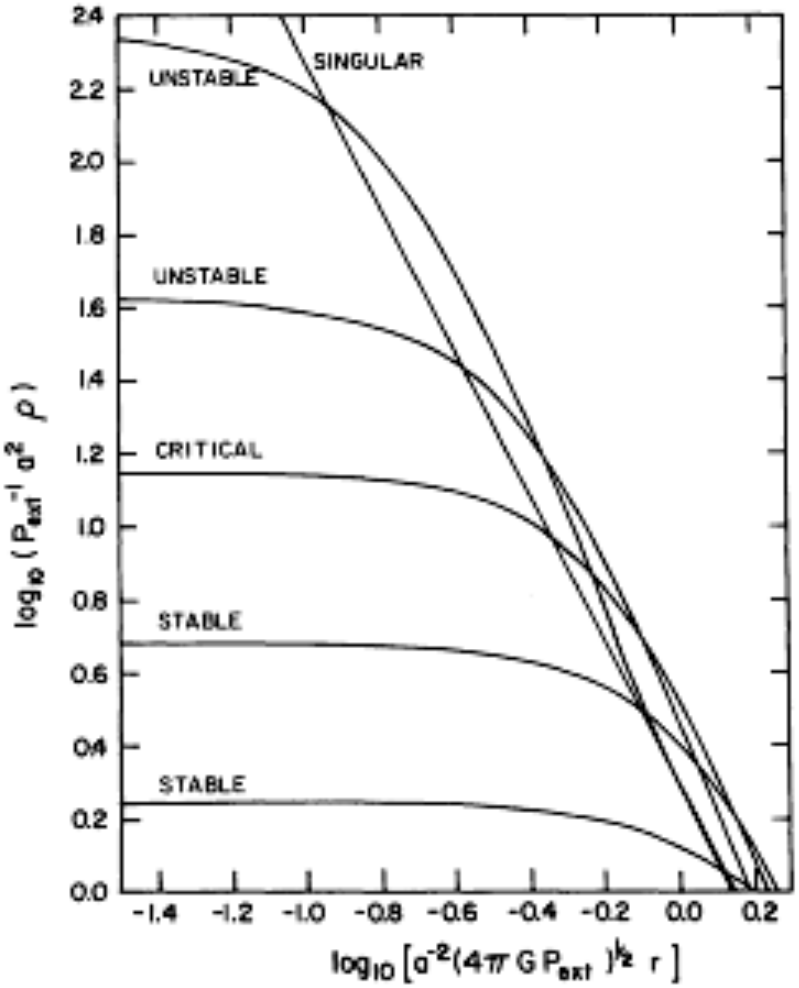

Stable and unstable equilibrium solutions of the BEM Eq.

Singular Solutions

Subsitute $\rho = A/r^2$ into

$$\frac{1}{r^2}\frac{d}{dr}\left(r^2\frac{1}{\rho}\frac{d\rho}{dr}\right)+\frac{4\pi G}{c^2}\rho=0 \quad \text{to get} \quad \frac{1}{r^2}\frac{d}{dr}(-2r)+\frac{4\pi G}{c^2}\frac{A}{r^2}=0$$

and find

$$\rho=\frac{c^2}{2\pi G}\frac{1}{r^2} \quad \text{and} \quad M(r)=\frac{2c^2}{G}r$$

These solutions are self-similar, i.e., they have no intrinsic spatial scale.

Shu took advantage of this property to find time-dependent solutions for the isothermal sphere using the scaled variables

$$x=r/ct, \qquad v=uc, \qquad \rho=\frac{\alpha(\mathrm{x})}{4\pi G t^2}, \qquad M(r,t)=\frac{c^3 t}{G}m(x)$$

Inside-Outside Collapse

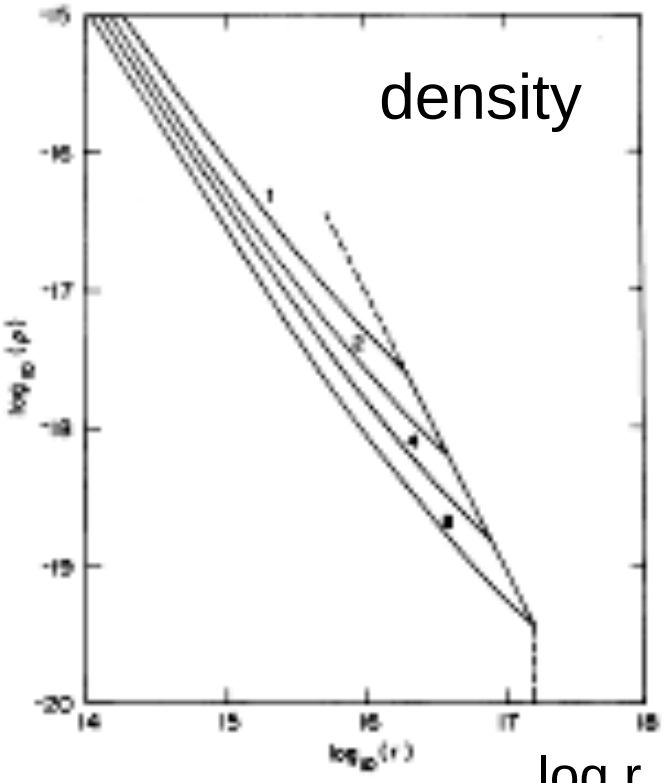

curves labeled by time in units of 30,000 yr

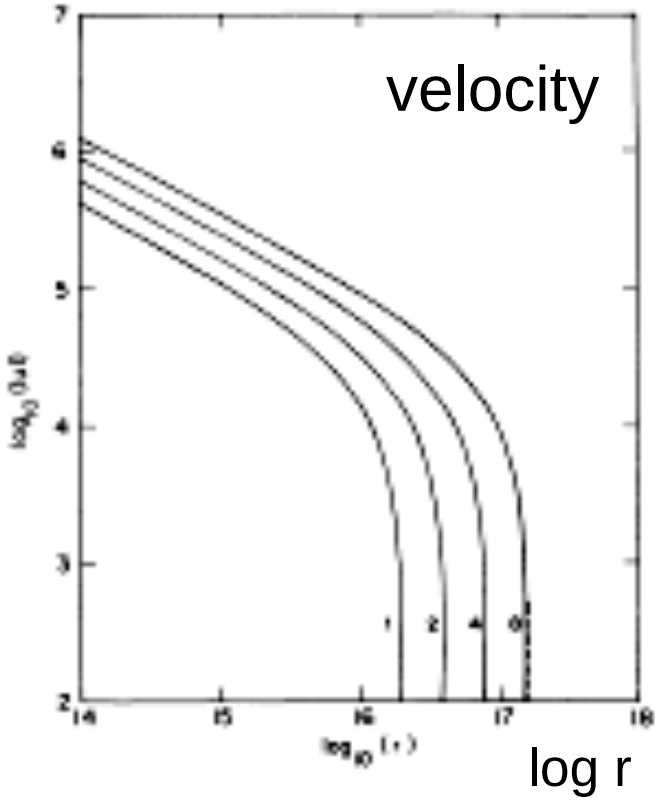

parameters: $M = 0.96\ M_{sun}$, $c = 0.2$ km/s, $P_{ext} = 1.1 \times 10^5$ K cm^{-3}

large $x = r/ct$: static solution for $r > ct$

small $x = r/ct$: free-fall collapse for $r < ct$

Singular Isothermal Sphere

Collapse at finite *r* occurs after the signal that collapse started at the center reaches *r*, *i.e.*, in time

$$t \approx \frac{r}{c} = 5.26\times10^5 \text{ yr}\left(\frac{r}{0.1\text{pc}}\right)\left(\frac{T}{10\text{K}}\right)^{-1/2}$$

It is of interest to account for the SIS mass distribution $M(r)$:

$$\text{accreted mass}: M(0^+) = \frac{c^3 t}{G} m_0$$

$$\text{infalling mass}: M(ct) - M(0^+) = \frac{c^3 t}{G}(2 - m_0)$$

$$\text{static envelope mass}: M(r) - M(ct) = \frac{2c^3 t}{G}\left(\frac{r}{ct} - 1\right)$$

The most remarkable result is that ***the accretion rate is determined only by the signal speed c and G***:

$$\dot{M}_{\text{acc}} = m_0 \frac{c^3}{G}$$

The parameter $m_0 = 0.975$

Final Remarks on the SIS

- The time for the mass with r to collapse is ~ the Jeans time for the average density within that sphere.

- Rotation will cut off the r^{-2} envelope beyond

$$R_C = \frac{c}{\Omega} \cong 1.86 \times 10^{17}\,\mathrm{cm} \left(\frac{10^{-13}\,\mathrm{rad\,s^{-1}}}{\Omega} \right) \left(\frac{T}{10\mathrm{K}} \right)^{1/2}$$

- The effects of magnetic fields have been studied in depth by Shu and collaborators, leading to ***singular isothermal toroids*** (SITs), e.g., Allen et al. ApJ 599 363 2003. Also see the work of Mouschovias and coworkers.

Final Remarks on the SIS

- The time for the mass with r to collapse is ~ the Jeans time for the average density within that sphere.

- Rotation will cut off the r^{-2} envelope beyond

$$R_C = \frac{c}{\Omega} \cong 1.86 \times 10^{17}\,\mathrm{cm} \left(\frac{10^{-13}\,\mathrm{rad\,s^{-1}}}{\Omega} \right) \left(\frac{T}{10\mathrm{K}} \right)^{1/2}$$

The final physical picture is a two component cloud core:

a collapsing inner region with $\rho \sim r^{-3/2}$ and $v \sim r^{-1/2}$

an outer static envelope with $\rho \sim r^{-2}$ and $v \sim$ constant

3. Observations of Collapse

It had been the hope of the early mm radio astronomers to discover molecular clouds in the process of collapse. They were rather surprised when, instead of collapse, *outflow* was discovered in the CO maps of the region around the YSO, L1551-IRS5 (next page), and later in hundreds of other sources.

Credible detections of infall were not made until the 1990s. The subject is reviewed by:

- Evans NJ II, ARAA 37 311 1999
- Myers, OSPS 1999
- Myers, Evans, & Ohashi, PPIV 2000, p. 217
- Evans 2002, astro-ph/0211526

The difficulty in analyzing optically thick lines continue to make this a controversial topic,

Discovery of Bipolar Molecular Outflows
Snell, Loren & Plambeck, ApJ 239 L17 1980

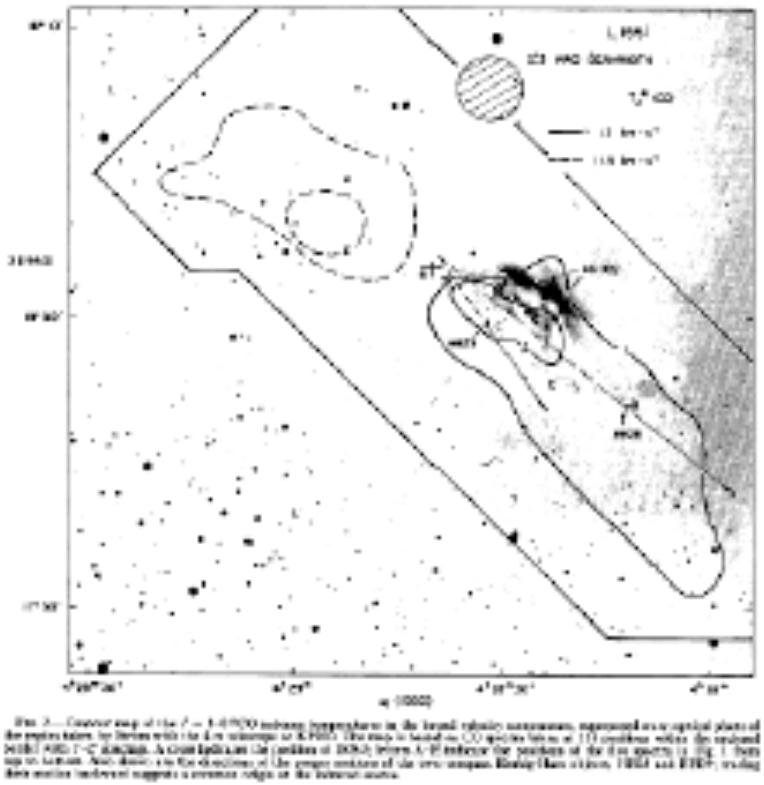

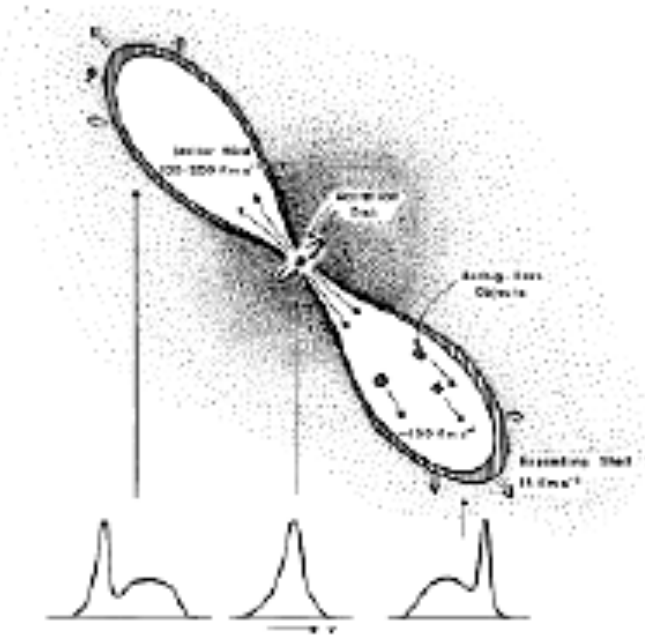

CO contours on an optical photo of the L1551-IRS5 region with H-H objects.

Paradigm-setting cartoon for the outflows from all low-mass YSOs.

One of Many Images Confirming The Snell, Loren, Plambeck Paradigm

HH-30 Disk & Jet (HST optical image)

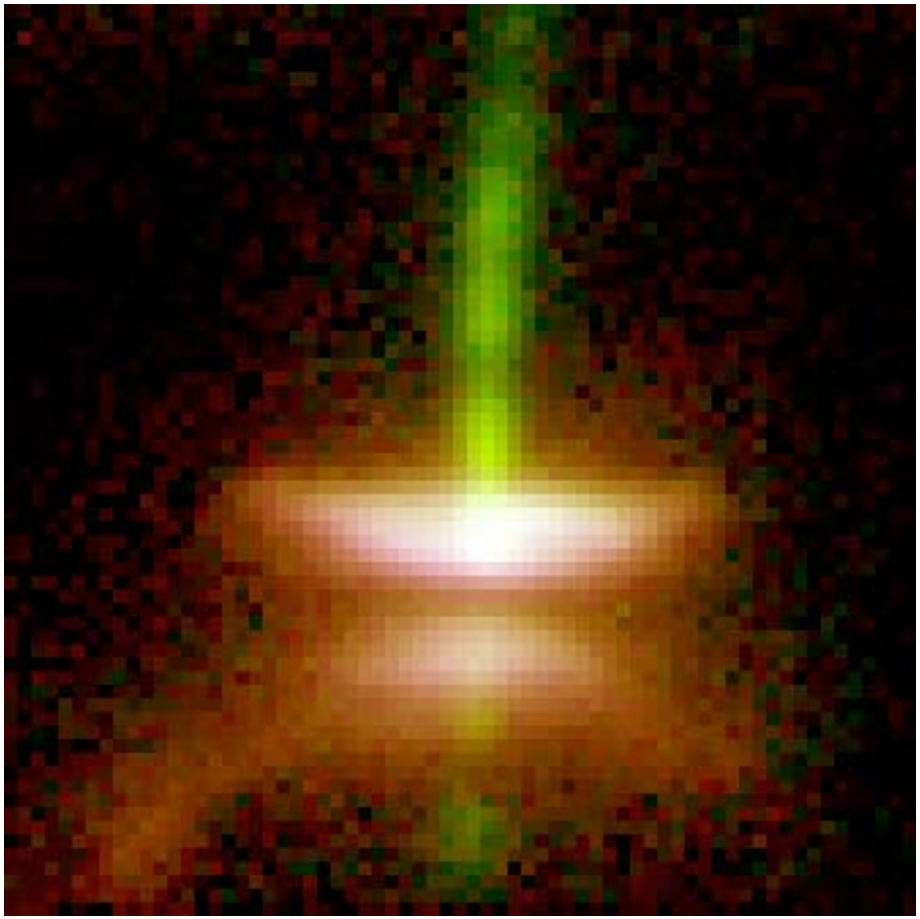

450 AU

Schematic for Infall Signature

Lada (1999)

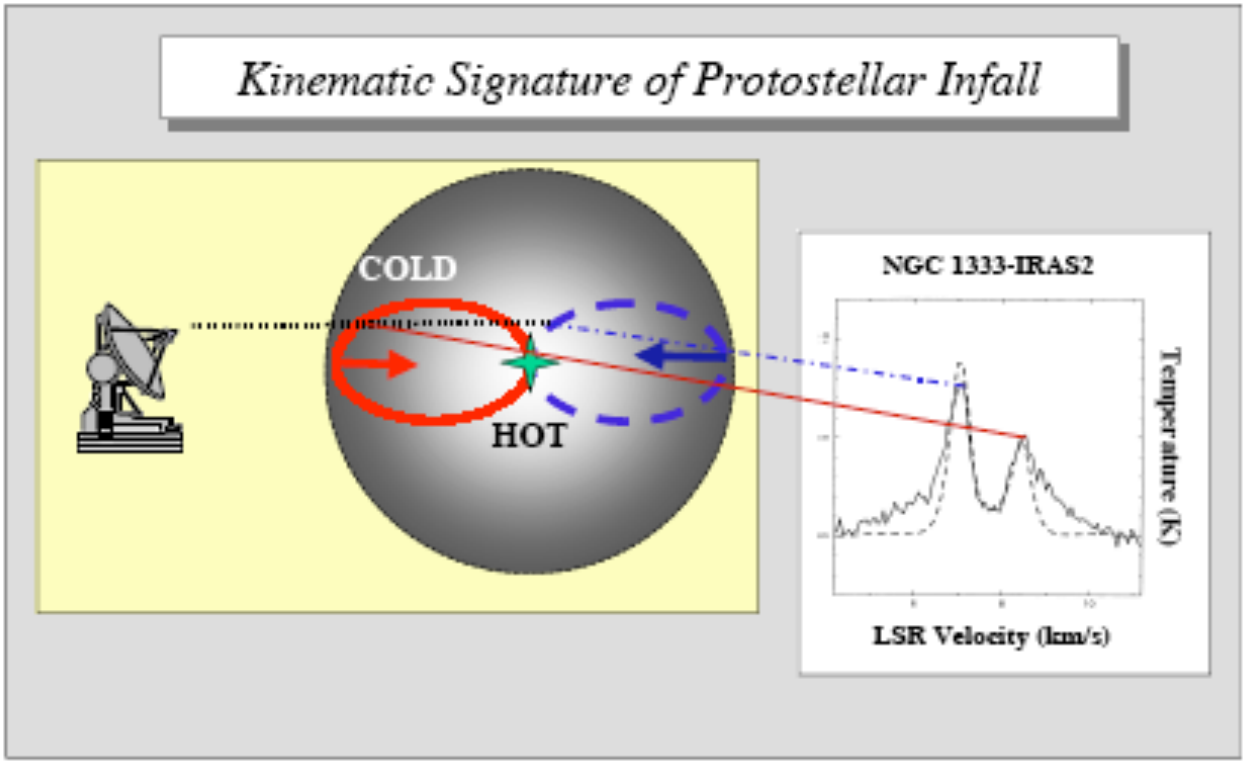

Figure 14. The kinematic signature of infall expected around a protostellar source. Oval curves represent lines of constant infall radial velocity. The dashed line represents blue-shifted gas, the solid line, red-shifted gas. Along a single line-of-sight the telescope beam intercepts the $\tau = 1$ surface in the outer, colder regions of the cloud at redshifted velocities and the inner hotter regions at blue-shifted velocites. The spectrum of NGC 1333-IRAS2 is from Ward-Thompson et al 1996.

Notice the assumption about locations of high/low excitation.

Alternate Schematic for Infall Signature

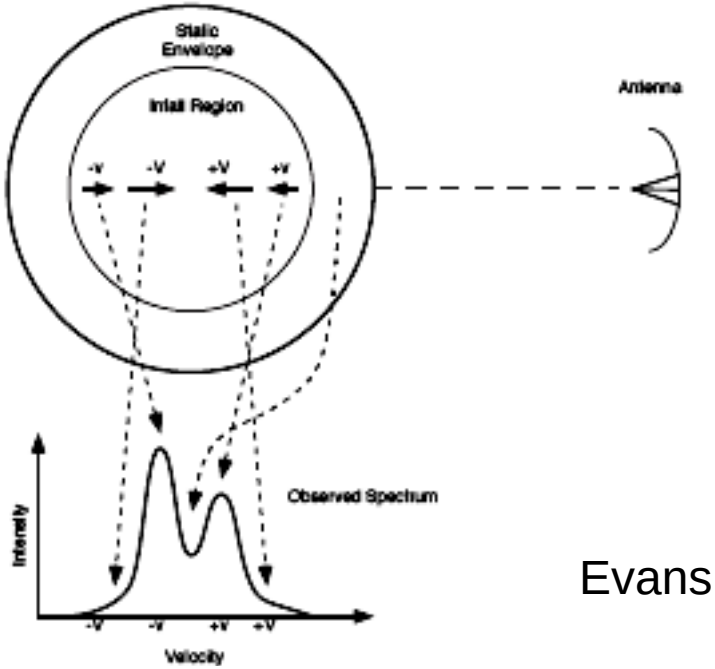

Evans ARAA 37 311 1999

Figure 1. The origin of various parts of the line profile for a cloud undergoing inside-out collapse. The static envelope outside r_{inf} produces the central self-absorption dip, the blue peak comes from the back of the cloud, and the red peak from the front of the cloud. The faster collapse near the center produces line wings, but these are usually confused by outflow wings.

Another Schematic for Infall Signature

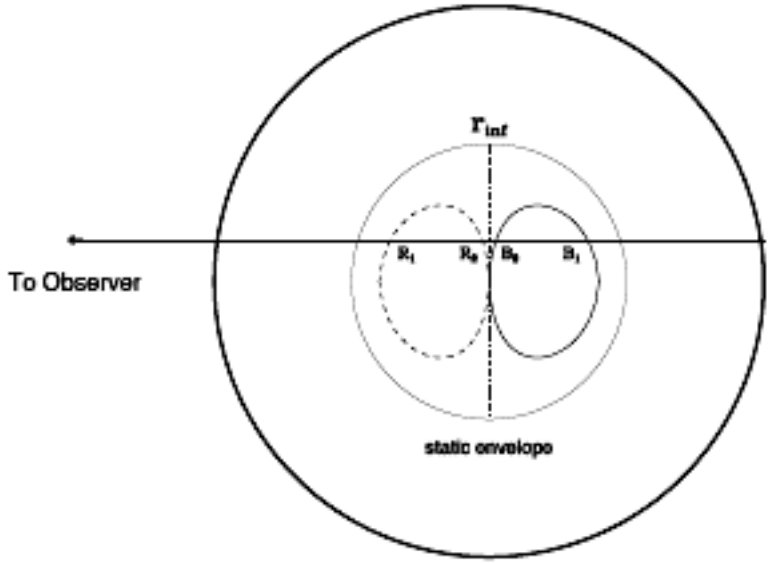

Evans ARAA 37 311 1999

Figure 2. A schematic explanation of why line profiles of optically thick, high-excitation lines are skewed to the blue in a collapsing cloud. The ovals are loci of constant line-of-sight velocity, for $v(r) \propto r^{-0.5}$. Each line of sight intersects these loci at two points. The point closer to the center will have a higher T_{ex}, especially in lines that are hard to excite, so that $T_{ex}(R_2) > T_{ex}(R_1)$ and $T_{ex}(B_2) > T_{ex}(B_1)$. If the line is sufficiently opaque, the point R_1 will obscure the brighter R_2, but B_2 lies in front of B_1. The result is a profile with the blue peak stronger than the red peak (Zhou & Evans 1994).

Myers Two-Slab Model

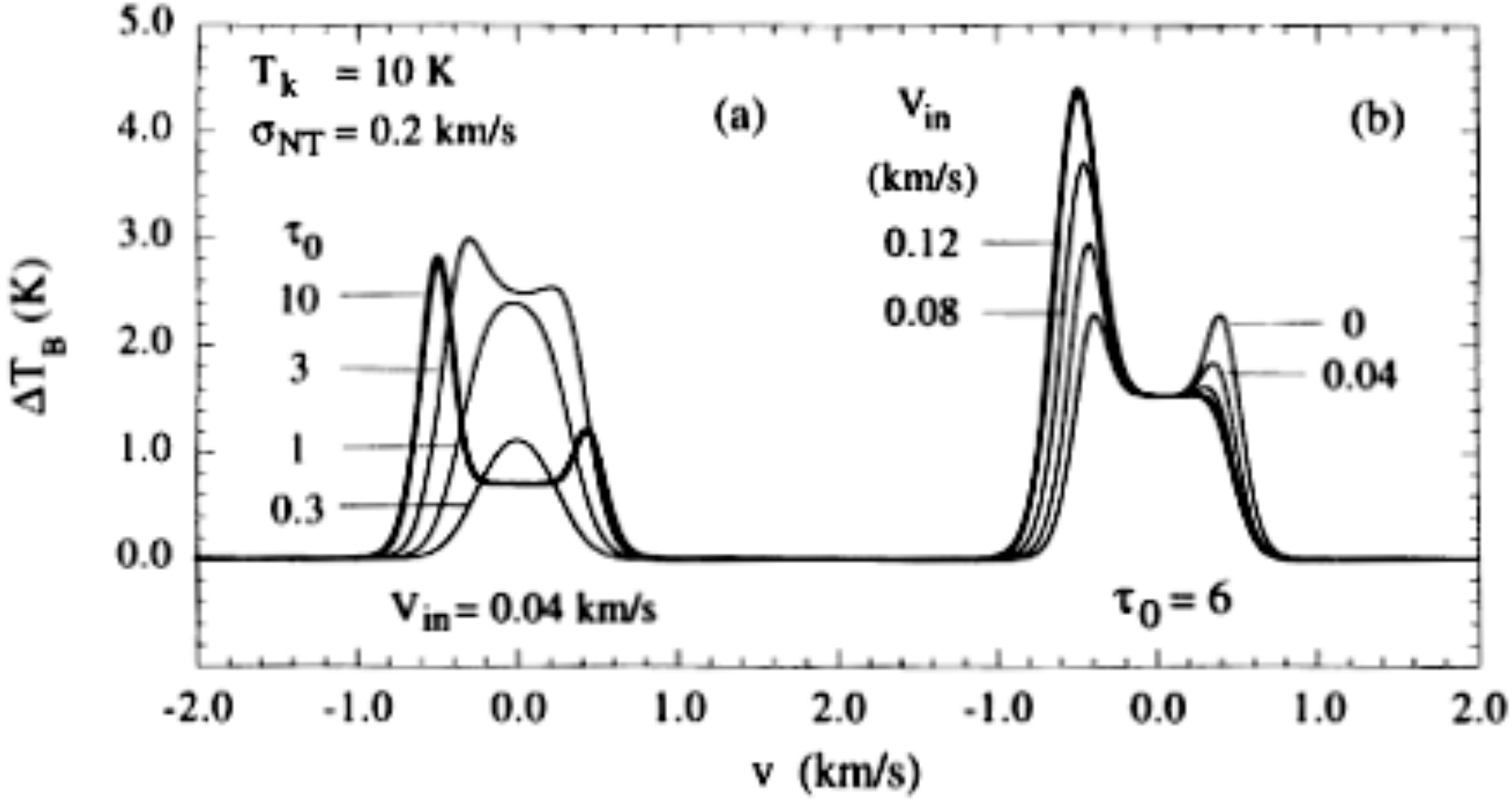

Effects of varying the optical depth and collapse speed.

B335: The Simplest Case

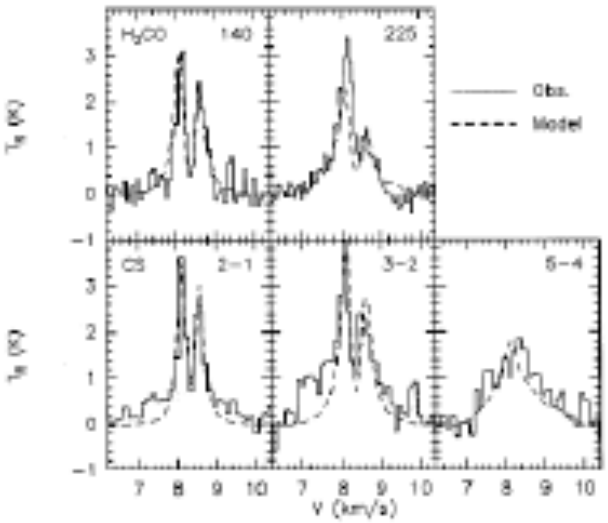

Figure 4 Line profiles of H_2CO and CS emission (solid histograms) toward B335 and the best-fitting model (dashed lines). The model line profiles were calculated with a Monte Carlo code, including non-LTE excitation and trapping, with an input density and velocity field taken directly from the collapse model of Shu (1977) and a temperature field calculated with a separate dust radiation transport code. The best-fitting model has an infall radius of 0.05 pc (Choi et al. 1995).

Choi et al. ApJ 448 742 1995
H_2CO & CS, with
critical densities ~ 10^6 cm^{-3}
dashed line is model

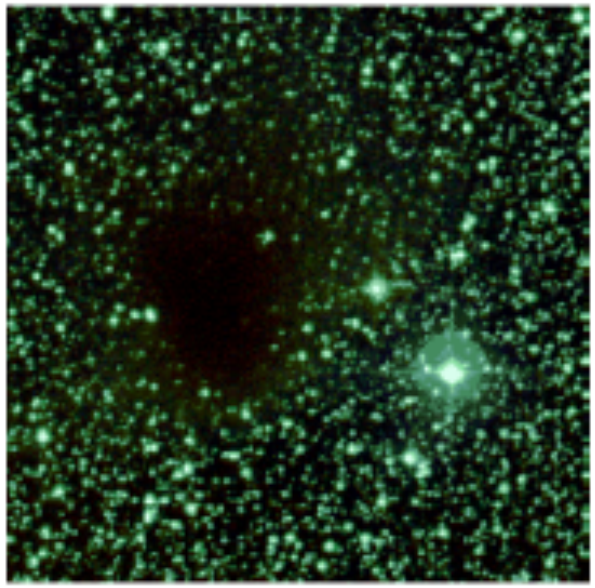

Figure 4.3: B335 global composite image from DSS2 survey. Red is DSS2-infrared, Green is DSS2-red and Blue is DSS2-blue. Image size is 9.8 X 9.8 arcminutes. North is up and East is left.

rounded Bok globule
distance ~ 250 pc
IRAS (> 60 m): L ~ 3 L_{sun}
many other mm lines
clumpy bipolar outflow

The Case of B335

Choi et al. (ApJ 442 742 1995) modeled the line shapes (shown on the previous page) using Shu's SIS by varying the temperature distribution, the CS & H_2CO abundances, and the beak point between the $r^{-3/2}$ and r^{-2} density distributions. They concluded that the observations support the inside-out collapse model.

But Wilner et al. (ApJ 544 L69 2000) observed the high-frequency 245 GHz CS(5-4) transition with the PdB interferometer at much higher angular resolution (3" instead of 11", corresponding to ~ 750 AU), and found a clumpy bipolar outflow & an inner off-center peak. The fit to the inside-out collapse model is degraded.

IRAM CS Observations of B335

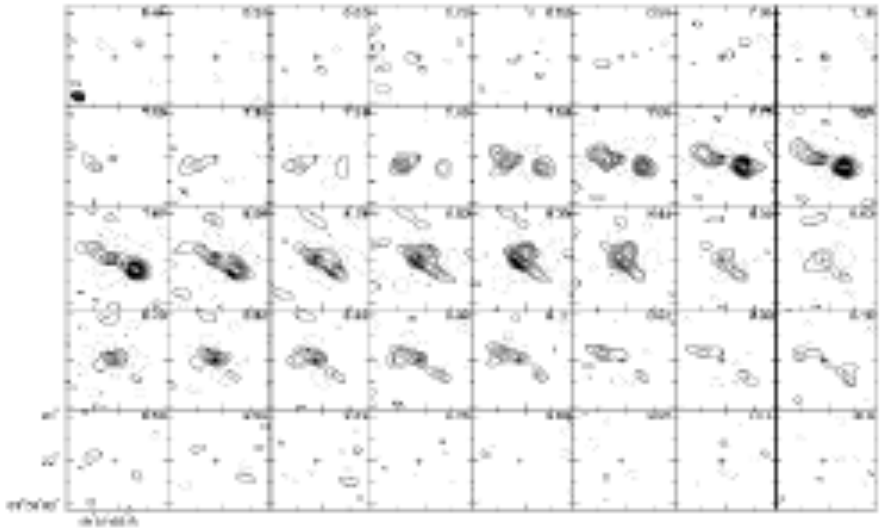

Interferometer channel maps showing outflow using CS(5-4)

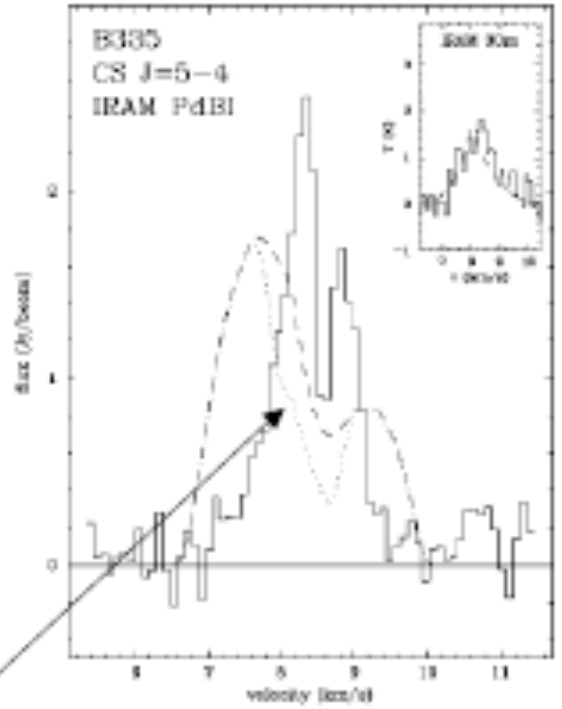

SIS modeling of line shape that includes fitting map data: dotted line

IRAM Dust Observations of B335

Harvey et al. (ApJ 596 383 2003) mapped the 1.2 & 3.0 mm continuum (dust) emission at a spatial resolution of 0.3" (10 times better than the previous CS(5-4) maps). They detect a disk-like structure of 100 AU and model the dust with an inside-outside density profile:

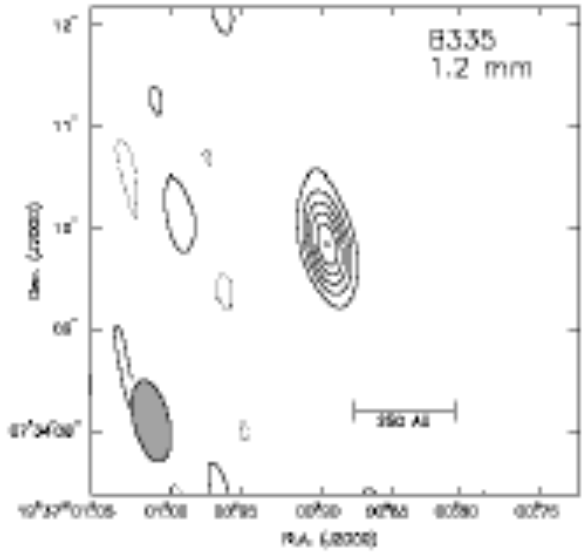

$$T = 10\mathrm{K}\left(r/5000\ \mathrm{AU}\right)^{-0.4} \text{ for } r < 5000\ \mathrm{AU} \text{ and } 10\mathrm{K} \text{ for } r > 5000\ \mathrm{AU}$$

$$\rho = \rho_0 \left(r / R_0\right)^{-p} \text{ for } r < R_0 \quad \text{and } \rho_0 \left(r / R_0\right)^{-2} \text{ for } R_0 < r < 25000\ \mathrm{AU}$$

They find p=1.55 +\- 0.04, R_0=6500 AU, $n_0(H_2)$=3.3x104 cm^{-3}, M(<6,500 AU) = 0.58 M_{sun} & M(<25,000 AU) = 3.06 M_{sun}, and argue for Shu's 1977 model.

Starless Core L1544

Tafalla et al. ApJ 504 9000 1998

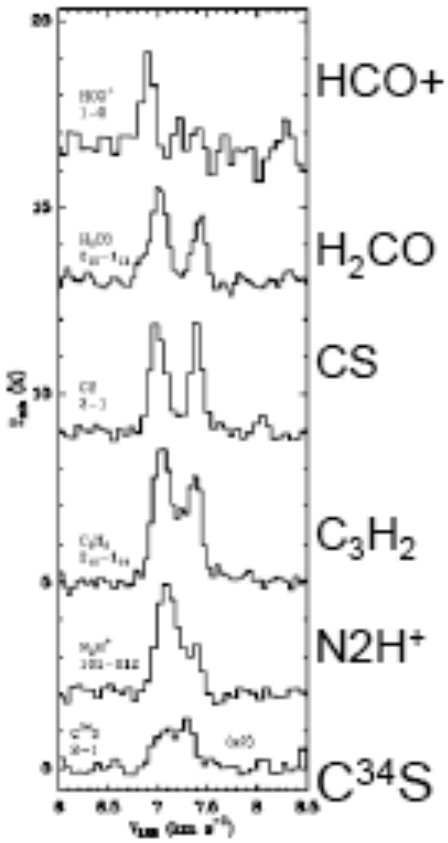

optically thick lines
opacity increasing upwards

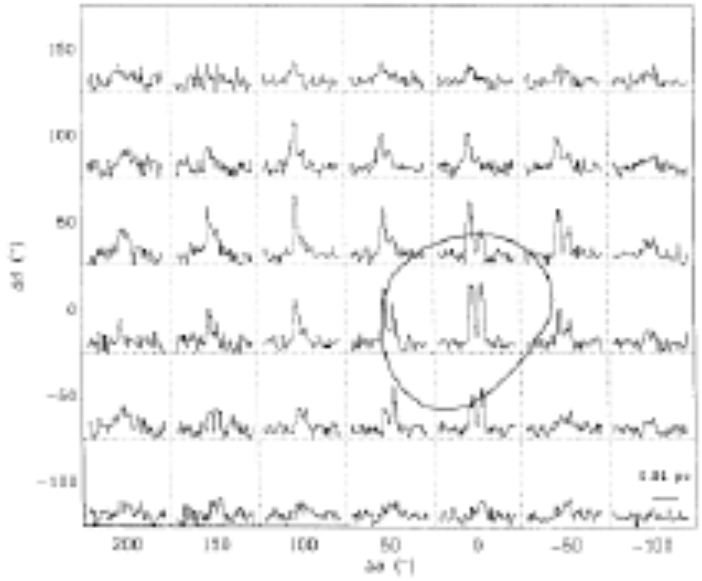

Figure 15. Map of profiles of the CS 2-1 line from the starless core L1544 in relation to the HII contour of the 1-0 line of N_2H^+, a tracer of dense core emission. The CS profiles show infall asymmetry extended over ~0.15 pc, much greater than the extent of the dense core (Tafalla et al 1998).

map of CS(2-1) profiles
asymmetry extends beyond N_2H^+ core
does not fit simple SIS models

Summary of Infall Signature Observations

- There is a basic problem to start: small infall velocity requires high spatial resolution observations.
- The line shape is affected by other dynamical motions, e.g., turbulence, rotation & outflow
- The analysis has to use good thermal, chemical & excitation models and deal with many lines reflecting different properties; dust also plays a role.
- The results depend on core shape and magnetic field.

- The observations probably do show infall, but the overall result is ambiguous, e.g., low resolution surveys yield many red-peaked profiles.
- ALMA is needed to go to the next level.